Computation and Visualization of Bifurcation Surfaces

Dirk Stiefs [a], Thilo Gross [b], Ralf Steuer [c] and Ulrike Feudel [a]

[a] *Theoretical Physics / Complex Systems, ICBM, Carl von Ossietzky University, PF 2503, 26111 Oldenburg, Germany*

[b] *Department of Chemical Engineering, Engineering Quadrangle, A-121, Princeton University, Princeton, NJ 08544-5263, USA*

[c] *University Potsdam, Institute of Physics, Nonlinear Dynamics Group, Am Neuen Palais 10,14469 Potsdam,Germany*

Abstract

The localization of critical parameter sets called bifurcations is often a central task of the analysis of a nonlinear dynamical system. Bifurcations of codimension 1 that can be directly observed in nature and experiments form surfaces in three dimensional parameter spaces. In this paper we propose an algorithm that combines adaptive triangulation with the theory of complex systems to compute and visualize such bifurcation surfaces in a very efficient way. The visualization can enhance the qualitative understanding of a system. Moreover, it can help to quickly locate more complex bifurcation situations corresponding to bifurcations of higher codimension at the intersections of bifurcation surfaces. Together with the approach of generalized models the proposed algorithm enables us to gain extensive insights in the local and global dynamics not only in one special system but in whole classes of systems. To illustrate this ability we analyze three examples from different fields of science.

Key words: Bifurcation, Visualization, Generalized Models, Codimension, Socio-Economic Model, Calcium Oscillations, Food Chain Model

1. Introduction

The long-term behavior of dynamical systems plays a crucial role in many areas of science. If the parameters of the system are varied, sudden qualitative transitions can be observed as critical points in parameter space are crossed. These points are called bifurcation points. The nature and location of bifurcations is of interest in many systems corresponding to applications from different fields of science. For instance the formation of Rayleigh-Bénard convection cells in hydrodynamics [Swinney & Busse, 1981], the onset of Belousov-Zhabotinsky oscillations in chemistry [Agladze & Krinsky,

Email address: stiefs@icbm.de (Dirk Stiefs).

1982, Zaikin & Zhabotinsky, 1970] or the breakdown of the thermohaline ocean circulation in climate dynamics [Titz et al., 2002, Dijkstra, 2005] appear as bifurcations in models. The investigation of bifurcations in applied research focusses mostly on codimension-1 bifurcations, which can be directly observed in experiments [Guckenheimer & Holmes, 1983]. In order to find bifurcations of higher codimension, in general at least two parameters have to be set to the correct value. Therefore, bifurcations of higher codimension are rarely seen in experiments. Moreover the computation of higher codimension bifurcations cause numerical difficulties in many models. Hence, an extensive search for higher codimension bifurcations is not carried out in most applied studies.

From an applied point of view the investigation of codimension-2 bifurcations is interesting, since these bifurcations can reveal the presence of global codimension-1 bifurcations–such as the homoclinic bifurcations–which are otherwise difficult to detect. The recent advances in the investigation of bifurcations of higher codimension are a source of many such insights [Kuznetsov, 1998]. While this source of knowledge is often neglected in applied studies, the investigation of bifurcations of higher codimension suffers from a lack of examples from applications [Guckenheimer & Holmes, 1983]. In this way a gap between applied and fundamental research emerges, that prevents an efficient cross-fertilization.

A new approach that can help to bridge this gap between mathematical investigations and real world systems is the investigation of generalized models. Generalized models describe the local dynamics close to steady states without restricting the model to a specific form, i.e. without specifying the mathematical functions describing the dynamics of the system [Gross et al., 2004, Gross & Feudel, 2006]. The computation of local bifurcations of steady-states in a class of generalized models is often much simpler than in a specific conventional model. A bifurcation that is found in a single generalized model can be found in every generic model of the same class. In this way the investigation of generalized models can provide examples of bifurcations of higher codimension in whole classes of models. From an applied point of view, it provides an easy way to utilize the existing knowledge on the implications of bifurcations of higher codimension on the dynamics.

For generalized models, the application of computer algebra assisted classical methods [Guckenheimer et al., 1997, Gross & Feudel, 2004] for computing bifurcations is advantageous. These methods are based on testfunctions for specific eigenvalue constellations corresponding to specific types of bifurcations [Seydel, 1991].

Classical methods yield implicit functions describing the mani-

folds in parameter space on which the bifurcation points are located. For codimension-1 bifurcations these manifolds are hypersurfaces. In order to utilize these advantages, an efficient tool for the visualization of implicitly described bifurcation hypersurfaces is needed. A properly adapted algorithm for curvature dependent triangulation of implicit functions can provide such a tool.

Generalized modeling, computer algebra assisted bifurcation analysis and adaptive triangulation are certainly interesting on their own. However, here we show that in combination they form a powerful approach to compute and visualize bifurcation surfaces in parameter space. This visualization yields also the relationship between the different bifurcations and identifies higher codimension bifurcations as intersections of surfaces. This way the proposed algorithm can help to bridge the present gap between applied and fundamental research in the area of bifurcation theory.

First, in Sec. 2. we briefly review how generalized models are constructed and how implicit test functions can be derived from bifurcation theory. In Sec. 3. we explain how these implicit functions can be combined with an algorithm of triangulation in order to visualize the bifurcations in parameter space. Finally in Sec. 4. we show three examples of generalized models from different disciplines of science. These illustrate how the proposed method efficiently reveals certain bifurcations of higher codimension and thereby provides qualitative insights in the local and global dynamics of large classes of systems.

2. Generalized Models and Computation of Bifurcations

The state of many real world systems can be described by a low dimensional set of state variables $X_1, \ldots, X_N$, the dynamics of which are given by a set of ordinary differential equations

$$\dot{X}_i = F_i(X_1, \ldots, X_N, p_1, \ldots, p_M), \quad i = 1 \ldots N \tag{1}$$

where $F_i(X_1, \ldots, X_N, p_1, \ldots, p_M)$ are in general nonlinear functions. For a large number of systems it is a priori clear which quantities are the state variables. Moreover, it is generally known by which processes the state variables interact. However, the exact functional forms by which these processes can be described in the model are often unknown. In practice, the functions in the model are often chosen as a compromise between empirical data, theoretical reasoning and the need to keep the equations simple. It is therefore often unclear if the dynamics that is observed in a model is a genuine fea-

ture of the system or an artifact introduced by assumptions made in the modeling process (e.g. [Ruxton & Rohani, 1998]).

One way to analyze models without an explicit functional form is provided by the method of generalized models [Gross & Feudel, 2006]. Since it will play an essential role in the examples discussed in Sec. 4., let us briefly review the central idea of this approach.

Let us consider the example of a system in which every dynamical variable is subject to a gain term $G_i(X_1, \ldots, X_N)$ and a loss term $L_i(X_1, \ldots, X_N)$. So that our general model is

$$F_i = G_i(X_1, \ldots, X_N) - L_i(X_1, \ldots, X_N) \tag{2}$$

Note that the parameters $(p_1, \ldots, p_M)$ do not appear explicitly, since the explicit functional form of the interactions G_i and L_i is not specified.

Since our goal is to study the stability of a nontrivial steady state, we assume that at least one steady state $\boldsymbol{X}^* = {X_1}^*, \ldots, {X_N}^*$ exists, which is true for many systems. Due to the fact that a computation of $\boldsymbol{X}^*$ is impossible with the chosen degree of generality we apply a normalization procedure with the aim to remove the unknown steady state from the equations. For the sake of simplicity we assume that all entries of the steady state are positive. We define normalized state variables $x_i = X_i/{X_i}^*$, the normalized gain terms $g_i(x) = G_i({X_1}^* x_1, \ldots, {X_N}^* x_N)/G_i(\boldsymbol{X}^*)$ as well as the normalized loss term $l_i(x) = L_i({X_1}^* x_1, \ldots, {X_N}^* x_N)/L_i(\boldsymbol{X}^*)$. Note, that by definition ${x_i}^* = g_i(\boldsymbol{x}^*) = l_i(\boldsymbol{x}^*) = 1$. Substituting these terms, our model can be written as

$$\dot{x_i} = (G_i(\boldsymbol{X}^*)/{X_i}^*) g_i(\boldsymbol{x}) - (L_i(\boldsymbol{X}^*)/{X_i}^*) l_i(\boldsymbol{x}). \tag{3}$$

Considering the steady state this yields

$$(G_i(\boldsymbol{X}^*)/{X_i}^*) = (L_i(\boldsymbol{X}^*) + /{X_i}^*). \tag{4}$$

We can therefore write our normalized model as

$$\dot{x_i} = \alpha_i (g_i(\boldsymbol{x}) - l_i(\boldsymbol{x})) \tag{5}$$

where $\alpha_i := G_i(\boldsymbol{X}^*)/{X_i}^* = L_i(\boldsymbol{X}^*)/{X_i}^*$ are scale parameters which denote the timescales - the characteristic exchange rate for each variable.

The normalization enables us to compute the Jacobian in the steady state. We can write the Jacobian of the system as

$$\mathbf{J}_{i,j} = \alpha_i (\gamma_{i,j} - \delta_{i,j}). \tag{6}$$

where we have defined

$$\gamma_{i,j} := \left.\frac{\partial g_i(x_1,\ldots,x_N)}{\partial x_j}\right|_{x=x^*} \tag{7}$$

and

$$\delta_{i,j} := \left.\frac{\partial l_i(x_1,\ldots,x_N)}{\partial x_j}\right|_{x=x^*} - \tag{8}$$

While the interpretation of $\gamma_{i,j}$ and $\delta_{i,j}$ describe the required information on the mathematical form of the gain and loss terms, we will see in Sec.4. that the parameters generally have a well defined meaning in the context of the application.

2.1. Testfunctions for bifurcations of steady states

Our aim is to study the stability properties of the steady state. Thus, only two bifurcation situations are of interest: (i) the loss of stability due to a bifurcation of saddle-node type where a real eigenvalue crosses the imaginary axis or (ii) a bifurcation of Hopf type where a pair of complex conjugate eigenvalues crosses the imaginary axis.

If a saddle-node bifurcation type occurs, at least one eigenvalue of the Jacobian $\mathbf{J}$ becomes zero. Therefore, the determinant of $\mathbf{J}$ is a test function for this bifurcation situation.

Hopf bifurcations are characterized by the existence of a purely imaginary complex conjugate pair of eigenvalues. We use the method of resultants to obtain a testfunction [Guckenheimer et al., 1997]. Since at least one symmetric pair of eigenvalues has to exist

$$\lambda_a = -\lambda_b. \tag{9}$$

The eigenvalues $\lambda_1,\ldots,\lambda_N$ of the Jacobian $\mathbf{J}$ are the roots of the Jacobian's characteristic polynomial

$$P(\lambda) = |\mathbf{J} - \lambda\mathbf{I}| = \sum_{n=0}^{N} c_n \lambda^n = 0. \tag{10}$$

Using condition (9) Eq. (10) can be divided (after some transformations) into two polynomials of half order

$$\sum_{n=0}^{N/2} c_{2n}\chi^n = 0, \tag{11}$$

$$\sum_{n=0}^{N/2} c_{2n+1}\chi^n = 0 \tag{12}$$

where $\chi = {\lambda_a}^2$ is the Hopf number and N/2 has to be rounded up or down to an integer as required.

In general two polynomials have a common root if the resultant vanishes [Gelfand et al., 1994]. The resultant R of Eq.(11) and Eq.(12) can be written as a Hurwitz determinant of size $(N-1) \times (N-1)$. If we assume that N is odd we have

$$R_N := \begin{vmatrix} c_1 & c_0 & 0 & \dots & 0 \\ c_3 & c_2 & c_1 & \dots & 0 \\ \vdots & \vdots & \vdots & \ddots & \vdots \\ c_N & c_{N-1} & c_{N-2} & \dots & c_0 \\ 0 & 0 & c_N & \dots & c_2 \\ 0 & 0 & 0 & \dots & c_2 \\ \vdots & \vdots & \vdots & \ddots & \vdots \\ 0 & 0 & 0 & \dots & c_{N-1} \end{vmatrix}. \tag{13}$$

With the condition $R_N = 0$ we have found a sufficient test function for symmetric eigenvalues. The Hopf number χ gives us the information whether the eigenvalues are real ($\chi > 0$), purely imaginary ($\chi < 0$), zero ($\chi = 0$) or a more complex situation (χ undefined). In the case $\chi = 0$ we have a double zero eigenvalue which corresponds to a codimension-2 Takens-Bogdanov bifurcation. In a Takens-Bogdanov bifurcation a Hopf bifurcation meets a saddle-node bifurcation. While the Hopf bifurcation vanishes in the TB bifurcation, a branch of homoclinic bifurcations emerges. For more details see [Gross & Feudel, 2004].

3. Visualization

The testfunctions, described above, yield an implicit description of the codimension-1 bifurcation hypersurfaces. Since it is in general not feasible to solve these functions explicitly we have to search for other means for the purpose of visualization. In the following we focus on the visualization in a three dimensional parameter space, in which the bifurcation hypersurfaces appear as surfaces. We propose an algorithm, that constructs the bifurcation surfaces from a set of bifurcation points, which have been computed numerically.

In order to efficiently obtain a faithful representation of the bifurcation surface the density of these points has to be higher in regions of higher curvature. Moreover, the algorithm has to be able

to distinguish between different - possibly intersecting - bifurcation surfaces.

3.1. Adaptive Triangulation

A triangulation is the approximation of a surface by a set of triangles. We apply a simplification of a method introduced by Karkanis & Stewart [2001] and extend it using the insights of the previous section. The algorithm consists of two main parts. The first is the *growing phase*, in which a mesh of triangles is computed that covers a large part of the surface. The second is the *filling phase*, in which the remaining holes in this partial coverage are filled.

3.2. The seed triangle

Denoting the three parameters as x, y and z, we start by finding one root $\mathbf{p}_1 = (x_1, y_1, z_1)$ of the testfunction, by a Newton-Raphson method (e.g. Kelley [2003]). Suppose $\mathbf{p}_1$ is a vertex of the *seed triangle*, then we search for two other points as two additional vertices that define a triangle of appropriate size and shape. We find another two roots $\mathbf{p}_{2\,\mathrm{initial}}$ and $\mathbf{p}_{3\,\mathrm{initial}}$ close to $\mathbf{p}_1$. $\mathbf{p}_{2\,\mathrm{initial}}$ and $\mathbf{p}_{3\,\mathrm{initial}}$ are within a radius of d_{initial} around $\mathbf{p}_1$ wherein the surface can be sufficiently approximated by a plane. We find the next vertex $\mathbf{p}_2$ using a point in the direction of $\mathbf{p}_{2\,\mathrm{initial}}$ with the distance d_{initial} to $\mathbf{p}_1$ as initial conditions for the Newton-Raphson method. The initial condition for the third vertex $\mathbf{p}_3$ is a point in the plane that is spanned by $\mathbf{p}_1$, $\mathbf{p}_{2\,\mathrm{initial}}$ and $\mathbf{p}_{3\,\mathrm{initial}}$, orthogonal to the line between $\mathbf{p}_1$ and $\mathbf{p}_2$, with a distance of d_{initial} to $\mathbf{p}_1$ as well. We get an almost isosceles seed triangle that approximates the bifurcation surface close to $\mathbf{p}_1$ sufficiently to our demands.

3.3. Growing phase

Starting from the seed triangle adjoining triangles can be added successively. The size of the adjoining triangles has to be chosen according to certain, possibly conflicting requirements. On the one hand the algorithm has to adapt the size of the triangles to the local surface curvature in order to obtain a higher resolution in regions of higher complexity and vice versa. On the other hand it has to maintain a minimal and a maximal resolution. At first we adapt the size of the triangle to the curvature of the surface.

We construct an interim triangle by mirroring $\mathbf{p}_1$ at the straight line through $\mathbf{p}_2$ and $\mathbf{p}_3$ and to find a point $\mathbf{p}_{4\,\mathrm{initial}}$ on the surface as shown in Fig.1. Thus $\mathbf{p}_{4\,\mathrm{initial}}$ defines together with $\mathbf{p}_2$ and $\mathbf{p}_3$ the interim triangle. The angle ϕ between the normals of the new

triangle and the parent is used to approximate the local radius of curvature. Following Karkanis & Stewart [2001] we define the radius of curvature as

$$R = \frac{d}{2sin\left(\frac{\phi}{2}\right)} \tag{14}$$

where d the distance of the centers of both triangles (cf. Fig. 1). We choose a desired ratio $\rho = R/d$ to compute a curvature adapted distance $d_{\text{adapt}} = R/\rho$. Finally we use again the Newton-Raphson method to find a bifurcation point $\mathbf{p}_4$ at the distance d_{adapt} from the straight line through $\mathbf{p}_2$ and $\mathbf{p}_3$ in the direction of $\mathbf{p}_{4\,\text{initial}}$. The bifurcation points $\mathbf{p}_2, \mathbf{p}_3$ and $\mathbf{p}_4$ then are the vertices of the adapted triangle. As mentioned above the adjacent triangles have to satisfy additional requirements. In order to maintain a minimal resolution we define a maximum $d_{\max}$. To restrict the number of computed bifurcation points we also define a minimum $d_{\min}$. If d_{adapt} is larger than $d_{\max}$ or smaller than $d_{\min}$ we set it to $d_{\max}$ or $d_{\min}$ respectively to find $\mathbf{p}_4$. To check the quality of the adapted triangle we also define a maximum angel $\phi_{\max}$. We decrease the distance d, if the angle between the normals of the triangles is greater than $\phi_{\max}$.

Proceeding as described above the algorithm adds to every triangle up to two adjacent triangles. In order to prevent overlapping triangles, we reject a triangle if its center is closer to the center of an opposite triangle than one and a half times the largest edge of both. To allow for self intersections of bifurcation surfaces (s. Sec.4.3.), we allow an intersection of triangles if the angle between the normals of the triangles is bigger than $2\phi_{\max}$. Another possibility which has to be taken into account is that our system may possess more than one bifurcation surface. To prevent transitions $\phi_{\max}$ has to be small enough. For instance, if two surfaces intersect at an angle $\hat{\phi}$, we have to choose $\phi_{\max}$ much smaller than $\hat{\phi}$. Concerning Hopf bifurcations the Hopf number χ offers a tool to distinguish between different surfaces, even if the angle of intersection is very small. Along one Hopf bifurcation surface χ varies smoothly. On a different Hopf bifurcation surface the Hopf number is in general different since another pair of purely imaginary eigenvalues is involved. We can therefore check the continuity of χ between the new bifurcation point and the parent to make sure that the new point belongs to the same surface.

Since the bifurcation surfaces are in general not closed, we have to restrict the parameter space according to a volume of interest V. We choose minimal and maximal values for each variable to define a cuboid which includes V. Triangles with vertices outside of the cuboid are rejected.

Apart from this restriction it is possible, that we find borders of the bifurcation surface within our cuboid. One example is a Hopf bifurcation surface that ends in a Takens-Bogdanov bifurcation as described in Sec.2. If we cross the Takens-Bogdanov bifurcation, the new point still can be settled down on the surface described by the test function. But in this case the Hopf number χ is positive and the symmetry condition is satisfied by a pair of purely real eigenvalues that is not related to a bifurcation situation. To place the new point directly onto the border of the Hopf bifurcation surface we compute the root of the χ-function using the coordinates of the new point as initial conditions. Then we use the resulting point again to find the root of our test function. Repeating this procedure we find iteratively our new point directly on the border of the Hopf bifurcation surface. In this way we can not only prevent a jump from one Hopf bifurcation surface to another one by checking the sign of χ, but we also approximate the border of the Hopf bifurcation surface.

Following the procedure described above we can successively add triangles to our mesh until no further triangle is possible. After the growing phase the complete surface, in the prescribed region of parameter space, is covered by a mesh of triangles as seen in the upper diagram in Fig.2.

3.4. Focus

Sometimes the bifurcation surfaces are quite smooth but in some regions they possess a more complicated structure. If the radius of curvature changes too rapidly the algorithm fails to adapt the size of the triangles and the structure is poorly approximated in this region. In these regions it is useful to increase the minimal resolution in order to obtain a more accurate approximation of the bifurcation surface. We realize this by so-called focus points. In a certain radius $\hat{r}$ around these focus points we reduse the maximal size of the triangles. The new maximal triangle size $\hat{d_{\max}}$ is then given as

$$\hat{d_{\max}} = \begin{cases} \left(c + \frac{(1-c)r}{\hat{r}}\right) d_{\max} & r < \hat{r} \\ d_{\max} & r \geq \hat{r} \end{cases}, \tag{15}$$

where r is the distance to the closest focus point and c is a constant between 0 and 1. By definition $\hat{d_{\max}}$ decreases linearly with r from $d_{\max}$ to a lower value $cd_{\max}$, where c is a constant between 0 and 1. In Fig. 2 we see a triangulation of an example surface after the growing phase. The upper diagram shows that two centers of a higher

resolution exit. The lower diagram shows that the surface looks like a landscape with a hill and a plane. One center of high resolution is on top of the hill and the other one in the plane. This example shows both resolution control mechanisms, the size adaption due to the radius of curvature (left) and due to a focus point (right).

While in Fig. 2 the focus point is not advantageous, this additional resolution control is essential for the computation of rather complicated bifurcation situations (s. Sec.4.).

3.5. Filling phase

While the growing phase covers a large fraction of the surface with connected traces of triangles, space between the traces remain. While we fill this gap, we have to take care that we do not fill space that lies outside the bifurcation surface, e.g. beyond a Takens-Bogdanov bifurcation. In the following we start by describing the filling phase for surfaces without boundaries and then go on to explain how boundaries are handled.

The first task we have to perform in the filling phase is to identify the gap. We can acquire the gap between the traces by starting at a vertex $\mathbf{p}_1$ and following the vertices at the boundary clockwise. In this way we construct a sequence of all N vertices.

Once we have defined a gap we start to separate the gap into subgaps. To each point of the gap we associate the normal $\mathbf{n}_k$ of an adjacent triangle and the closest neighbor. Similar to Karkanis & Stewart [2001] we define all points as neighbors of $\mathbf{p}_k$ which are located between the two half planes which are spanned by the normal $\mathbf{n}_k$ and the two vectors from $\mathbf{p}_k$ to $\mathbf{p}_{k-1}$ and $\mathbf{p}_{k+1}$ shown in Fig. 3(a). The closest neighbor of $\mathbf{p}_k$ is the neighbor with the smallest Euclidian distance. If we find two points, which are the closest neighbors to each other they form a so-called *bridge*. We divide the gap at the first bridge we find into two subgaps by connecting the two vertices. If a subgap consists of only three vertices, we add it as a triangle to the mesh we obtained from the growing phase. We proceed with the subgaps as described above until no bridges are left. Afterwards we divide the remaining subgaps at the point with the smallest distance to its closest neighbor. In the end of this procedure the hole gap is completely filled up with triangles.

3.6. Borders in the filling phase

If the bifurcation surfaces are not closed but possess some boundaries due to margins of the parameter region under consideration, or due to a codimension-2 bifurcation e.g. a Takens Bogdanov bi-

furcation then we have gaps which are not supposed to be filled up. In order to prevent bridges connecting these borders, we use similar criteria for the bridges and all connections we make to divide the gaps, as used in the growing phase.

First, the connections the algorithm produces by the division of gaps should not be much larger than $d_{\max}$ to preserve a minimal resolution. In order to prevent long connections at the margins of the parameter region we look for closest neighbors in a radius of $3d_{\max}$. In order to prevent triangles with edges longer than $2d_{\max}$, we choose the maximal connection length as $1.8d_{\max}$. If a connection is longer, we compute an additional point on the surface close to the middle of the bridge and take this additional point into account. This criterion may also prevent the filling of an area where the bifurcation condition is not satisfied. This is particularly true in case of a Hopf bifurcation if the Hopf number χ is positive at this point. As described above the algorithm would automatically try to find a bifurcation point at the border of the Hopf bifurcation surface. If the computation of the new bifurcation point fails the division is denied.

Second, the angles between the resulting triangles and the triangles of the mesh should not be larger than $\phi_{\max}$. This criterion keeps the triangulation smooth and may prevent the covering of a more complex region of the surface. Let ϕ_i and ϕ_j denote the angles between the connection and the normals $\mathbf{n}_i$ and $\mathbf{n}_j$ associated to the connected vertices as shown in Fig.3(b). Further, we denote ϕ_{n} as the angle between the two normals $\mathbf{n}_i$ and $\mathbf{n}_j$ (see Fig.3(c)). If the difference from ϕ_i and ϕ_j to 90 degrees is larger than $\phi_{\max}$ or ϕ_{n} is larger than $\phi_{\max}$, we compute an additional point between as well. As illustrated in Fig.3(d) a new point in the connection will in general cause a kink. If the angle of the kink in the connection is bigger than $\phi_{\max}$, the division is denied. If we can not compute the new point, because probably the bifurcation does not exist close to it, the division is also rejected.

Having obtained an adaptive triangulation of the bifurcation surface, we have to consider how to display the set of triangles.

3.7. Level lines

One the one hand visualization of the edges of the triangles can lead to visual fallacies. Small triangles seem to be far away while large triangles may look very close. Focus points sometimes exacerbate this effect. On the other hand not displaying only the triangle surface without edges would deprive the viewer of clues on the three dimensional shape of the surface. We introduce level lines as a cos-

metic tool. Like the level lines in a map we project certain values from the axes onto the surface.

Finally we demonstrate the ability of our algorithm by the computation of a Whitney umbrella type bifurcation surface which may appear as a higher codimension bifurcation for Hopf bifurcations (cf. Sec.4.3.). In this case the bifurcation surface is twisted in itself (cf. Fig.4). Even close to the end of the intersection line, where the crossing angle becomes small, no transitions occur. While in most regions the degree of curvature is quite small, a sharp edge appears close to the end of the line where the Hopf bifurcation intersects itself. Since the radius of curvature decreases rapidly at this edge from a quite high value to a very small one, the adaptive resolution control would fail to adapt the size of the triangles in this region. However, using focus points close to the end of the crossing line we can prevent bigger gaps in this region.

After the filling phase is completed (Fig. 4(b)) we cut off the outer triangles in order to obtain even margins at the boundary of the region in parameter space. Instead of the triangles we display now the level lines on the surface for both horizontal axes in Fig. 4(b). As mentioned above not only the bifurcation surfaces but also the intersection lines are of interest since they form bifurcations of higher codimension. In order to highlight these bifurcations we finally mark the intersection line and its endpoint as shown in Fig. 4(d).

4. Examples

In order to demonstrate the wide applicability of our algorithm let us now consider three examples from different disciplines of science. We start with a socio-economic model and continue with a metabolic network as well as a food chain model from population dynamics

4.1. Bifurcation analysis of a generalized socio-economic model

While the history of China is characterized by periodic transitions between despotism and anarchy the European dynasties exhibit stable behavior for extended periods of time. A simple model describing the interaction of three different parts of the society, namely farmers X_1, bandits X_2 and rulers X_3 can predict such dynastic cycles as well as steady state behavior. The specific model has been investigated in Feichtinger et al. [1996], Gross & Feudel [2006] studied a generalized version of this model. The generalized model is given as

a system of three differential equations

$$\begin{aligned} \dot{X}_1 &= S(X_1) - C(X_1, X_2) - T(X_1, X_3), \\ \dot{X}_2 &= \eta C(X_1, X_2) - L(X_2, X_3) - M(X_2), \\ \dot{X}_3 &= \nu C(X_1, X_2) - R(X_3), \end{aligned} \tag{16}$$

where η and ν are constant factors.

For the sake of clearness we refer to the individual processes by different letters and not by different indices as we have done in Sec.2. The function $S(X_1)$ denotes the gain or growth terms of the farmers which already includes natural mortality. The loss terms $C(X_1, X_2)$ and $T(X_1, X_3)$ which reduce the population of farmers represent crime and taxes respectively. Because the population of bandits benefits from crime the function $C(X_1, X_2)$ multiplied with a constant factor η which denotes the gain term of the bandits. The rulers benefit from crime as well, because crime increases the willingness of farmers to support the rulers. Therefore, the number of rulers grows also proportional to $C(X_1, X_2)$ with a constant factor ν. The rulers reduce the number of bandits by fighting crime. This effect is taken into account by the term $L(X_2, X_3)$. Finally the mortality of the bandits and the rulers is expressed by the terms $M(X_2)$ and $R(X_3)$ separately.

The normalization procedure from Sec. 2. that leads to the scaling and generalized parameters is shown in detail in [Gross & Feudel, 2006]. Here we focus on the computation ond visalization of the bifurcaation surfaces in order to illustrate the advantages of the proposed method. The steady state can undergo saddle-node and Hopf bifurcations (Fig. 5). The considered parameter space is spanned by 3 parameters. The first parameter β_1 (β_x in [Gross & Feudel, 2006]) is a scaling parameter of the normalized model. It is the ratio of farmer losses due to crime and the total farmer losses in the steady state. It tends to one if the losses of farmers due to crime is much lager than the losses due to taxes. The parameters s_1 and c_2 (s_x and c_y in [Gross & Feudel, 2006]) are so called generalized parameters. They appear in the Jacobian of the normalized model as the derivatives of the normalized processes in the steady state like $\gamma_{i,j}$ and $\delta_{i,j}$ in Sec. 2.. In that sense they are a measure of the nonlinearity of the corresponding process. As it has been noted they can be interpreted in the context of the model under consideration. For instance s_1 corresponds to $\lambda_{1,1}$ in Sec. 2. and is defined as the derivative of the normalized term $s(x_1) = S({X_1}^* x_1)/S({X_1}^*)$ with respect to x_1 in the steady state. However, we can take it as a measure of available land. If there is plenty of usable land available, the productivity

Term $S(X_1)$ is expected to be proportional to the number of farmers X_1. In this case the parameter s_1 is one. By contrast, if there is a shortage of usable land s_1 approaches zero. In a similar way, the derivative c_2 of the normalized term $c(x_1, x_2)$ with respect to x_1 may symbolize the autonomy of the bandits in the steady state. If the bandits do neither constrain each other nor cooperate c_2 is equal to one. While in case of competition between the bandits c_2 is expected to be smaller than one. These interpretations allow us to obtain a qualitative understanding of the results of our bifurcation analysis.

The red surface in Fig. 5 is a manifold of Hopf bifurcation points and the slightly transparent blue surface is a manifold of bifurcation points of saddle-node type. The steady state is stable in the top-most volume on the right side of the parameter space and unstable everywhere else in the diagram. Starting from any point within the stable volume an increase of β_1 causes the crossing of the Hopf surface at a certain value. At this point the stability is lost and a limit cycle occurs. This transition can be understood as a change from a stable dynasty to dynastic cycles. In that sense the parameter β_1 and therefore a domination of crime in farmer losses tends to destabilize the system.

While the shape of the surfaces helps to understand the (de-)stabilizing effects of the bifurcation parameters, the intersections of these surfaces (dashed lines) give informations about other bifurcations to be expected in the system and about the global dynamics of the system. Our diagram contains two such lines. The almost vertical dashed line marks a Takens-Bogdanov bifurcation (TB) line which is characterized by two zero eigenvalues. As we know from Sec. 2., at least one homoclinic bifurcation has to emerge from the Takens-Bogdanov bifurcation. The horizontal dashed line marks a cross section of the surface of Hopf bifurcations and the surface of generalized saddle-node bifurcations, where we find a zero eigenvalue in addition to a purely imaginary pair of complex conjugate eigenvalues. This codimension-2 bifurcation is a Gavrilov-Guckenheimer (GG) bifurcation [Gavrilov, 1980, Guckenheimer, 1981] which arises from a so called triple-point bifurcation with a triple zero eigenvalue. A homoclinic bifurcation emerges from the Gavrilov-Guckenheimer bifurcation as well. In addition, a Neimark-Sacker bifurcation which is related to the emergence of quasiperiodic motion can be found. Due to these additional bifurcations in the neighborhood of the Gavrilov-Guckenheimer bifurcation, parameter regions of quasiperiodic dynamics exist and chaos is likely to occur. As Fig. 5 shows these regions are expected to occur at moderate values of s_1 and at relatively high values of β_1. By contrast, at low values of β_1 no

such regions can be found. Thus we can conclude that a domination of crime in farmer losses tends not only to destabilize the system locally but may also lead to quasiperiodic and chaotic dynamics.

4.2. Bifurcation Analysis of a Model of Intracellular Calcium Oscillations

Similar to the socio-economic system considered above, the fundamental biochemical processes that take place in living cells cannot be understood without recourse to mathematical modeling. Thus recently the concept of generalized models was extended to incorporate the specific structural properties of cellular metabolism to describe and elucidate the possible dynamics of metabolic and biochemical systems [Steuer et al., 2006].
To exemplify the computation and visualization of bifurcation surfaces in generalized models of cellular regulation, we consider a minimal model of intracellular calcium oscillations. Though strictly speaking not a genuine metabolic system, calcium ions (Ca^{2+}) are an ubiquitous intracellular messenger and are involved in the regulation and control of numerous cellular processes [Berridge et al., 2000]. Periodic temporal variation in the intracellular concentration of calcium is known for a long time and is observed in a large variety of different cell types [Berridge et al., 2000, Schuster et al., 2002]. Furthermore, due to the universality and the importance in intracellular signaling, the analysis of calcium oscillations has been accompanied by mathematical modeling almost from the beginning [Schuster et al., 2002]. In particular the observation of more complex forms of self-sustained calcium oscillation, such as bursting and chaotic temporal behavior, triggered an eminent interest in the analysis of the local and global bifurcations that arise in minimal and more elaborate models of intracellular calcium dynamics [Schuster et al., 2002].
Following a previously proposed model of calcium dynamics [Houart et al., 1999, Goldbeter et al., 2001], consisting of 3 concentration variables and 6 reaction and transport fluxes, we restrict our analysis to the key processes depicted in Fig. 6: Cells mobilize cytoplasmic Ca^{2+} from internal, as well as external sources. Internal stores are held within various intracellular compartments, most dominantely the endoplasmatic reticulum (ER). Release of Ca^{2+} is controlled by inositol 1,4,5-triphosphate ($InsP_3$), as well as by the cytoplasmic Ca^{2+} concentration itself (calcium-induced calcium release, CICR). Given the model structure depicted in Fig. 6, the system can be represented by a set of 3 differential equations, corresponding to the time dependent concentrations of cytoplasmic calcium Ca^{2+}_{cyt} (X_1),

available calcium in the store Ca^{2+}_{store} (X_2), and cytoplasmic inositol 1,4,5-triphosphate (X_3). The respective differential equations are then defined by the product of the 3×6 dimensional stoichiometric matrix $\boldsymbol{N}$ and the (as yet unspecified) 3-dimensional vector of rate equations $\boldsymbol{K}(\mathbf{X})$, describing the dependence of the reaction rates and transport processes on the respective concentrations.

$$\frac{\mathrm{d}}{\mathrm{d}t}\begin{bmatrix} X_1 \\ X_2 \\ X_3 \end{bmatrix} = \mathbf{N}\boldsymbol{K}(\mathbf{X}) = \begin{bmatrix} +1 & -1 & +1 & -1 & 0 & 0 \\ 0 & 0 & +1 & -1 & 0 & 0 \\ 0 & 0 & 0 & 0 & +1 & -1 \end{bmatrix} \begin{bmatrix} K_1 \\ K_2(X_1) \\ K_3(X_1, X_2, X_3) \\ K_4(X_1) \\ K_5 \\ K_6(X_1, X_3) \end{bmatrix} \quad (17)$$

Using the generalized approach described previously [Steuer et al., 2006], the information contained in Eq. (17) is already sufficient to fully specify a parametric representation of the Jacobian matrix of the normalized system.

$$\boldsymbol{J_x} := \boldsymbol{\Lambda\theta^{\mu}_{x}} = \begin{bmatrix} \alpha_1 & -\alpha_1 & +\alpha_2 & -\alpha_2 & 0 & 0 \\ 0 & 0 & +\alpha_3 & -\alpha_3 & 0 & 0 \\ 0 & 0 & 0 & 0 & +\alpha_4 & -\alpha_4 \end{bmatrix} \cdot \begin{bmatrix} 0 & 0 & 0 \\ \theta^2_1 & 0 & 0 \\ \theta^3_1 & \theta^3_2 & \theta^3_3 \\ \theta^4_1 & 0 & 0 \\ 0 & 0 & 0 \\ \theta^6_1 & 0 & \theta^6_3 \end{bmatrix} \quad (18)$$

In this parametric representation of the Jacobian, the elements of the 3×6 dimensional matrix $\boldsymbol{\Lambda}$ correspond the (inverse) characteristic timescales of the reaction and transport processes and are fully specified by the stoichiometry of the system and the (often experimentally accessible) steady state concentrations $\boldsymbol{X^*}$ and steady state flux values $\boldsymbol{K^*} = \boldsymbol{K}(\boldsymbol{X^*})$.

$$\alpha_1 := \frac{K^*_1}{X^*_1} \qquad \alpha_2 := \frac{K^*_3}{X^*_1} \qquad \alpha_3 := \frac{K^*_3}{X^*_2} \qquad \alpha_4 := \frac{K^*_5}{X^*_3} \quad (19)$$

The elements of the 6×3 dimensional matrix $\boldsymbol{\theta^{\mu}_{x}}$ are defined as the partial derivatives of the (normalized) rate functions with respect

to the (normalized) concentration variables at the steady state $\boldsymbol{X}^*$.

$$\theta_i^j := \left.\frac{\partial k_j(\boldsymbol{x})}{\partial x_i}\right|_{\boldsymbol{x}^*=\mathbf{1}} \qquad \text{with} \qquad k_j := \frac{K_j(\boldsymbol{X})}{K_j(\boldsymbol{X}^*)} \quad \text{and} \quad x_i := \frac{X_i}{X_i^*} \tag{20}$$

As demonstrated previously [Steuer et al., 2006], each element θ_i^j measures the normalized degree of saturation of a reaction K_j with respect to a metabolite X_i at the steady state $\boldsymbol{X}^*$ and can be assigned to a well-defined interval, even when the explicit functional form of the respective rate equation is not known. For example, export of calcium to the extracellular medium, as described by the transport reaction $K_2(X_1)$, depends only on cytoplasmic calcium concentration $\mathrm{Ca}^{2+}_{\mathrm{cyt}}$ (X_1). The second row in $\boldsymbol{\theta}^{\boldsymbol{\mu}}_{\boldsymbol{x}}$ thus only contains a single positive nonzero entry in the first column $\theta_1^2 \in [0,1]$, corresponding to the (normalized) saturation of the export reaction $K_2(X_1)$ with respect to its substrate X_1. Similar, release of Ca^{2+} from the internal store by the transport reaction $K_3(\boldsymbol{X})$ depends on the available calcium in the store X_2, thus $\theta_2^3 > 0$. Additionally the export reaction K_3 is activated by cytoplasmic calcium $\mathrm{Ca}^{2+}_{\mathrm{cyt}}$ (X_1) and InsP_3 (X_3), thus the respective saturation parameters are $\theta_1^3 \in [0,n]$ and $\theta_3^3 \in [0,n]$, where n denotes a positive integer describing the cooperativity of the reaction.

Equation (18), together with its interpretation in biochemical terms, now allows for a systematic analysis of the characteristic bifurcations of the Jacobian matrix, without the need to specify the explicit functional form of any of the involved rate equations [Steuer et al., 2006]. Figure 7 depicts a bifurcation diagram of the model as a function of 3 generalized saturation parameters. As in the previous sections, the red surface displays a manifold of Hopf bifurcations and the slightly transparent blue surfaces are manifolds of generalized saddle-node bifurcations. Similar to the first example, the steady state is stable in the top right volume of the diagram. If we cross one of the surfaces the stability is lost. For this reason, increasing the saturation of calcium release with respect to cytoplasmic calcium, thus decreasing the saturation parameter θ_1^3, inevitably leads to a loss of stability. If the value of θ_2^3 is low, this loss of stability is related to a Hopf bifurcation. This means that either an unstable limit cycle vanishes or a stable limit cycle occurs. The latter case explains the commonly observed calcium oscillations.

However, as has been noted above, most interest today focuses on the explanation of more complex dynamics. It has been shown that special models of the form of Eq.(17) can account for complex intracellular $\mathrm{Ca}^{\mathbf{2}+}$ oscillations [Borghans et al., 1997, Goldbeter et al., 2001, Houart et al., 1999]. The question is wether these dynamics

result only from the more or less arbitrary assumptions about the exact functional form of the rate equations $\boldsymbol{K}$, or whether they result from more elementary properties of the system, such as the stoichiometry and the assumed regulatory interactions. The advantage of the generalized model, and hence of our conclusions about possible dynamics, is that these are independent from the former: The localization of bifurcations of higher codimension provides the desired information on global dynamics, independent of the exact functional form of any of the involved rate equations. Figure 7 shows that the Hopf bifurcation surface emerges from and ends in a Takens-Bogdanov bifurcation line. The two lines where this surface crosses the generalized saddle-node bifurcation surfaces are Gavrilov Guckenheimer bifurcation lines. Again, as described in Sec.4.1. this shows the existence of quasiperiodic and chaotic parameter regions in the model close to the GG lines. While in Fig. 7 the parameter θ_3^3 only varies within the range $[0, 1]$ the model discussed by Houart et al. [1999] allows a maximum value of 4. However, the GG lines can be found in the whole range except for small values of θ_3^3. Here, the GG lines vanish at the TB lines in triple point bifurcations. As a variety of global bifurcations is located in the neighborhood of these triple point bifurcations, we can expect the richest dynamics in this region.

4.3. Bifurcation analysis of a general food chain model

Our last example is a generalized four-trophic food chain model. Each trophic level n may correspond to one species or to a group of similar species X_{n}. The first level X_1 is called primary producer and the last level X_4 is named top predator. A generalized model of such food chains is given in Gross [2004] which can be written in the four-trophical case as

$$\begin{aligned}
\dot{X}_1 &= S(X_1) - F_1(X_1, X_2), \\
\dot{X}_2 &= \eta_2 F_1(X_1, X_2) - F_2(X_2, X_3), \\
\dot{X}_3 &= \eta_3 F_2(X_2, X_3) - F_3(X_3, X_4), \\
\dot{X}_4 &= \eta_4 F_3(X_3, X_4) - M(X_4),
\end{aligned} \tag{21}$$

where the term $S(X_1)$ denotes the primary production which is assumed to depend on X_1 and $M(X_4)$ describes the mortality of the top predator. The biomass loss of species X_i due to predation by species X_{i+1} is given as $F_i(X_i, X_{i+1})$ where $i = 1..3$ and η_{i+1} describes the fraction of biomass predation that is converted into biomass of the predator. While $S(X_1)$ could also include natural

mortality of the primary producer (apart from predation) we assume that predation is much higher than natural mortality. As a result we neglect the natural mortality of species X_2 and X_3. According to the procedure described in Subsection 2. the normalized model of (21) can be written as

$$\begin{aligned} \dot{x_1} &= \alpha_1(s(x_1) - f_1(x_1, x_2)), \\ \dot{x_2} &= \alpha_2(f_1(x_1, x_2) - f_2(x_2, x_3)), \\ \dot{x_3} &= \alpha_3(f_2(x_2, x_3) - f_3(x_3, x_4)), \\ \dot{x_4} &= \alpha_4(f_3(x_3, x_4) - m(x_4)), \end{aligned} \tag{22}$$

where we can identify α_n, $n = 1 \ldots 4$ again as inverse timescale parameters. Following Gross et al. [2004] we assume an allometric slowdown of the timescales described by the ratio $r = \alpha_{n+1}/\alpha_n < 1$. Applying a normalization of time we can set $\alpha_1 = 1$ and $\alpha_n = r^{n-1}$. Thereby we express all scaling parameters by the parameter r that describes the timescale separation. Another bifurcation parameter we use is the sensitivity to prey $\gamma_n := \partial f_n(x_n, x_{n+1})/\partial x_n$, $n = 1 \ldots 3$. If prey x_n is abundant the parameter γ_n will approach zero. It is larger if prey is scarce and equal to one if predation is proportional to prey density. As Gross [2004] pointed out, the value of γ_n depends strongly on the feeding strategy of predator x_{n+1}.

In the four-trophic food chain the steady state loses its stability in a Hopf bifurcation. As shown in Fig. 8 the surface of Hopf bifurcations possesses a rather complicated shape. It turns out that the four trophic food chain is one of the rare examples of applications that exhibits a Whitney umbrella type bifurcation, used in Sec. 3. to illustrate the capabilities of the algorithm presented. It is formed around a codimension-3 1:1 resonant double Hopf bifurcation at the end of the line of double Hopf bifurcations (DH) of codimension 2. It has been shown that chaotic parameter regions generally exist close to a double Hopf bifurcation [Kuznetsov, 1998].

The parameter range in which the 1:1-resonant double Hopf bifurcation occurs can only be reached if the predation rates can be described by Holling type-III predator-prey interaction [Holling, 1959]. However, such interactions are frequently observed in nature. To our knowledge, this is the first example of a 1:1-resonant double Hopf bifurcation that was found in an applied model. Moreover, the existence of the bifurcation in the generalized model shows that this bifurcation can generically be found in a large class of four throphic food chains. Generalized models of longer food chains and more complex food webs often exibit multiple 1:1-resonant double Hopf

bifurcations.

5. Discussion

In this paper we have proposed and applied a combination of generalized modeling, bifurcation theory and adaptive triangulation techniques. This approach has enabled us to compute and visualize the local codimension-1 bifurcation hypersurfaces of steady states. In order to obtain a faithful representation of the surface at a low computational cost the algorithm automatically adapts the size of the computed triangle elements to the local complexity of the surface. Due to the application of generalized modeling, the resulting bifurcation diagrams do not describe a single model, but a class of models that share a similar structure.

The proposed approach enables the researcher to rapidly compute three parameter bifurcation diagrams for a given class of models. By considering several of these diagrams with different parameter axes an intuitive understanding of the local dynamics in a given class of systems can be gained. In particular, the approach bridges the gap between applied and fundamental research as discussed in the Introduction. In the visualization of local bifurcations as surfaces in a three dimensional parameter space, certain local bifurcations of higher codimension can be easily spotted. In our experience the proposed approach reveals bifurcations of codimension two and three in almost every model studied. It thereby provides plentiful examples for mathematical analysis. In return insights gained from the investigation of higher-codimension bifurcations can directly feed back in the investigation of the system. In particular the implications of local bifurcations of higher codimension, discussed above, is intriguing in this context. Provided that the dynamical implications of a bifurcation are known from normal form theory, the appearance of such a bifurcation in the three parameter diagram, pinpoints a parameter region of interesting dynamics. This region can then be investigated in conventional models or experiments. In this way the investigation of models is facilitated by reducing the need for more costly parameter search in conventional models.

In the present paper we have only used the proposed approach in conjunctions with testfunctions for two basic local bifurcations: the Hopf bifurcation and the saddle-node bifurcation. However, in principle, the approach can be extended to include testfunctions for codimension-2 bifurcations. This would allow the algorithm to adaptively decrease the size of triangles close to these bifurcations and continue the bifurcation lines directly once they are reached.

Furthermore, being hyperlines, the codimension-2 bifurcation points form surfaces in a four dimensional parameter space. Once again these surfaces can be triangulated with the described algorithms. The four dimensional space could be visualized in a movie, where time represents the forth parameter or by collapsing and color coding one of the parameter dimensions. Both approaches would allow for the visual identification of bifurcations of codimension three and higher.

At present the proposed approach has two limitations. First, the extraction of information is solely based on the Jacobian. Higher orders, which determine the normal form coefficients, are at present not taken into account. However, parameters that capture this information could be defined in analogy to the exponent parameters, which we have used to capture the required information on the nonlinearity of the equations of motion.

The second limitation is that the approach outlined here is presently only applicable to systems of small or intermediate dimension ($N < 10$) as the analytical computation of the testfunctions becomes cumbersome for larger systems. This problem can be avoided by combining the triangulation techniques proposed here with the numerical investigation of generalized models demonstrated in [Steuer et al., 2006].

References

Agladze, K. I. & Krinsky, V. I. [1982] "Multi-armed vortices in an active chemical medium," *Nature* **296**, 424 – 426.

Berridge, M. J., Lipp, P. & Bootman, M. D. [2000] "The versality and universality of calcium signalling," *Nature Reviews Molecular Cell Biology* **1**, 11–12.

Borghans, J. A. M., Dupont, G. & Goldbeter, A. [1997] "Complex intracellular calcium oscillations: A theoretical exploration of possible mechanisms," *Biophysical Chemistry* **66**, 25–41.

Dijkstra, H. A. [2005] *Nonlinear Physical Oceanography*, 2nd ed., vol. 28 of *Atmospheric and Oceanographic Sciences Library*. (Springer-Verlag, Berlin, Heidelberg, New York).

Feichtinger, G., Forst, C. V. & Piccardi [1996] "A nonlinear dynamical model for the dynastic cycle," *Chaos Solutions & Fractals* **7**, no. 2, 257–271.

Gavrilov, N. [1980] "On some bifurcations of an equilibrium with two pairs of pure imaginary roots," in *Methods of Qualitative*

Theory of Differential Equations (GGU, USSR), pp. 17–30. in russian.

Gelfand, I. M., Kaprov, M. M. & Zelevinsky, A. V. [1994] *Discriminants, Resultants and Multidimensional Determinants*. (Birkhäuser, Boston).

Goldbeter, A., Gonze, D., Houart, G., Leloup, J.-C., Halloy, J. & Dupont, G. [2001] "From simple to complex oscillatory behavior in metabolic and genetic control networks," *Chaos* **11**, no. 1, 247–260.

Gross, T. [2004] *Population Dynamics: General Results from Local Analysis*. (Der Andere Verlag, Tönningen, Germany).

Gross, T., Ebenhöh, W. & Feudel, U. [2004] "Enrichment and foodchain stability: the impact of different forms of predator-prey interaction," *Journal of Theoretical Biology* **227**, 349–358.

Gross, T. & Feudel, U. [2004] "Analytical search for bifurcation surfaces in parameter space," *Physica D* **195**, no. 3-4, 292–302.

Gross, T. & Feudel, U. [2006] "Generalized models as a universal approach to nonlinear dynamical systems," *Physical Review E* **73**, no. 016205. (14 pages).

Guckenheimer, J. [1981] "On a codimension two bifurcation," *Lecture Notes in Mathematics* **898**, 99–142.

Guckenheimer, J. & Holmes, P. [1983] *Nonlinear Oscillations, Dynamical Systems, and Bifurcations of Vector Fields*, 1st ed., vol. 42 of *Applied Mathematical Siences*. (Springer-Verlag, Berlin, Heidelberg, New York).

Guckenheimer, J., Myers, M. & Sturmfels, B. [1997] "Computing Hopf bifurcations I," *SIAM J. Numer. Anal.* **34**, no. 1, 1.

Holling, C. S. [1959] "Some characteristics of simple types of predation and parasitism," *The Canadian Entomologist* **91**, 385–389.

Houart, G., Dupont, G. & Goldbeter, A. [1999] "Bursting, chaos and birhythmicity originating from self-modulation of the inositol 1,4,5-triphosphate signal in a model for intracellular Ca^{2+} oscillations," *Bull. of Math. Biol.* **61**, 507–530.

Karkanis, T. & Stewart, A. J. [2001] "Curvature-dependent triangulation of implicit surfaces," *IEEE Computer Graphics and Applications* **22**, no. 2, 60–69.

Kelley, C. T. [2003] *Solving Nonlinear Equations with Newton's Method (Fundamentals of Algorithms).* (SIAM, Philadelphia).

Kuznetsov, Y. A. [1998] *Elements of Applied Bifurcation Theory*, 2nd ed., vol. 112 of *Applied Mathematical Siences.* (Springer-Verlag, Berlin, Heidelberg, New York).

Ruxton, G. D. & Rohani, P. [1998] "Population floors and persistance of chaos in population models," *Theoretical Population Biology* **53**, 75–183.

Schuster, S., Mahrl, M. & Höfer, T. [2002] "Modelling of simple and complex calcium oscillations: From single-cell responses to intercellular signalling," *Eur. J. Biochem.* **269**, 1333–1355.

Seydel, R. [1991] "On detecting stationary bifurcations," *International Journal of Bifurcation and Chaos* **1**, no. 2, 335–337.

Steuer, R., Gross, T., Selbig, J. & Blasius, B. [2006] "Structural kinetic modeling of metabolic networks," *Proc Natl Acad Sci U S A* **103**, no. 32, 11868–11873.

Swinney, H. L. & Busse, F. H. [1981] *Hydrodynamic instabilities and the transition to turbulence.* (Springer-Verlag, Berlin, Heidelberg, New York).

Titz, S., Kuhlbrodt, T. & Feudel, U. [2002] "Homoclinic bifurcation in an ocean circulation box model," *International Journal of Bifurcation and Chaos* **12**, no. 4, 869–875.

Zaikin, A. N. & Zhabotinsky, A. M. [1970] "Concentration wave propagation in two-dimensional liquid-phase self-oscillating system," *Nature* **225**, 535 – 537.

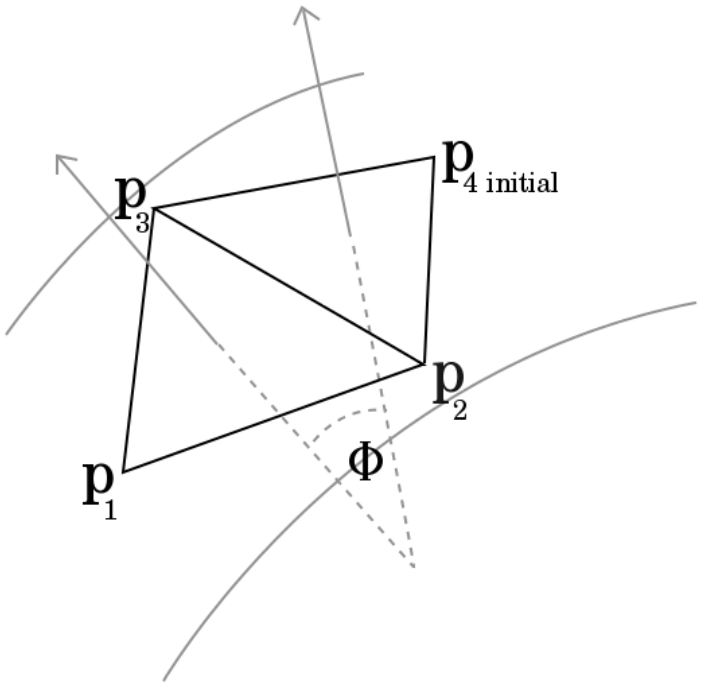

Figure 1: Seed triangle with one adjacent triangle.

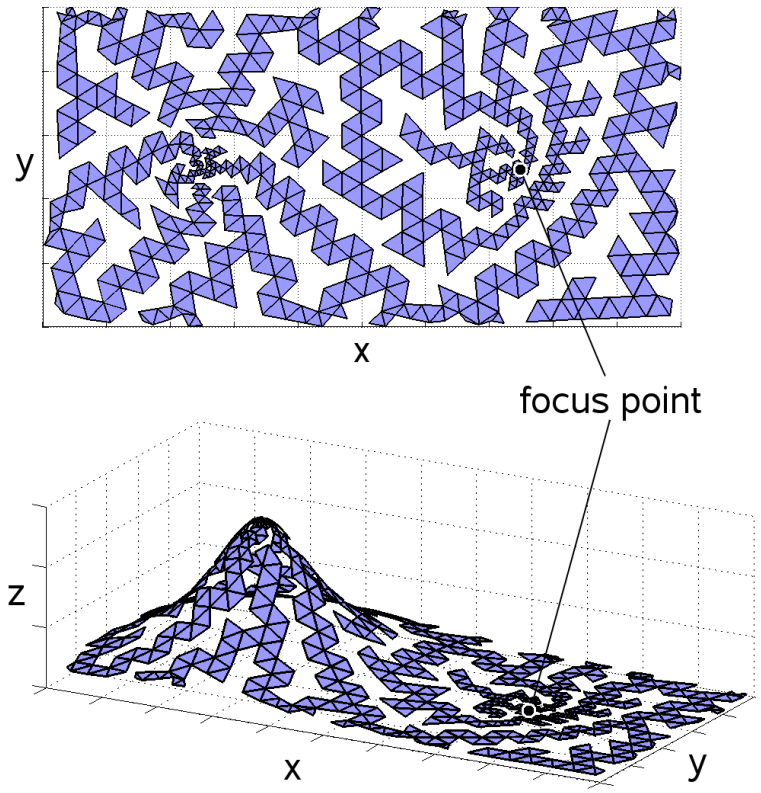

Figure 2: Example surface after the growing phase computed with one focus point. The size of the triangles adapts to the local curvature and the proximity to the focus point.

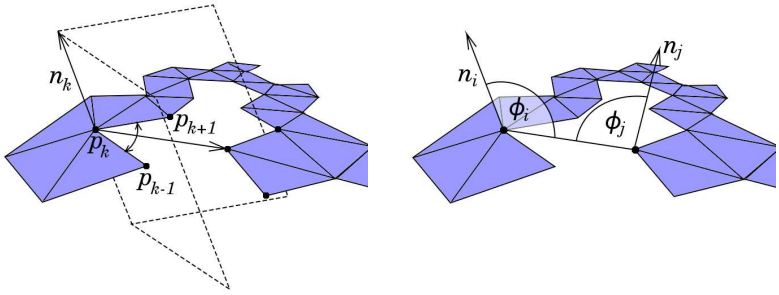

(a) The space of possible neighbors of $\mathbf{p}_k$ is within the two half planes spanned by the normal $\mathbf{n}_k$ associated to $\mathbf{p}_k$ and the two vectors from $\mathbf{p}_k$ to $\mathbf{p}_{k-1}$ and $\mathbf{p}_{k+1}$.

(b) The difference between the angles ϕ_i and ϕ_j to 90 degrees has to be less than $\phi_{\max}$

(c) The angle ϕ_n between the normals of the connected points has to be less than $\phi_{\max}$

(d) If an additional point in the middle of the bridge is necessary the angle ϕ_{kink} has to be less then $\phi_{\max}$

Figure 3: A connection in the filling phase is called bridge and has to satisfy different conditions.

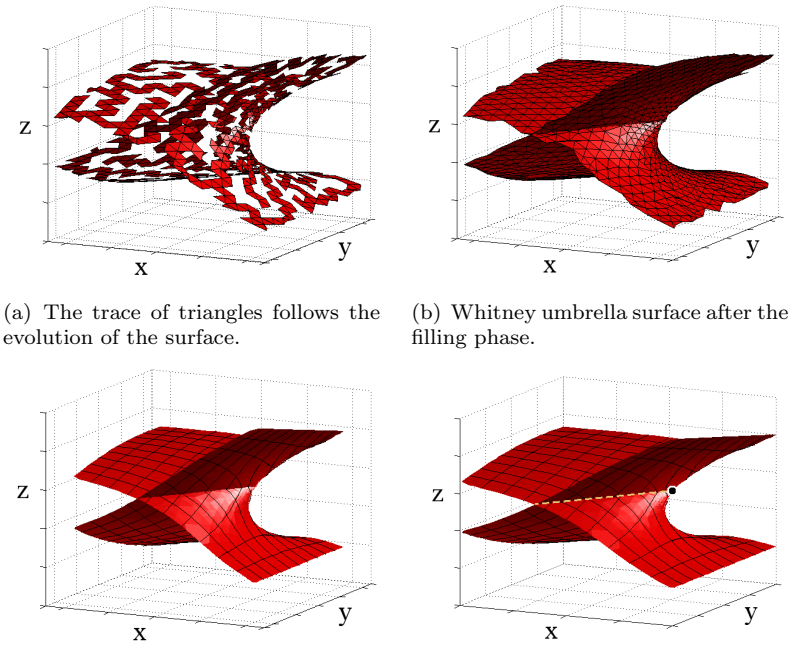

(a) The trace of triangles follows the evolution of the surface.

(b) Whitney umbrella surface after the filling phase.

(c) Whitney umbrella surface after the filling phase with level lines (no highlighting of the triangle edges).

(d) Marking of intersection line and its endpoint

Figure 4: Construction of a bifurcation diagram that shows a Hopf bifurcation surface possessing the shape of a Whitney umbrella. This bifurcation is found in a population dynamical system given in Sec. 4.3. While the upper subplots (a) and (b) show the two phases of the triangulation algorithm, the lower subplots (c) and (d) illustrate the preparation of the resulting diagram.

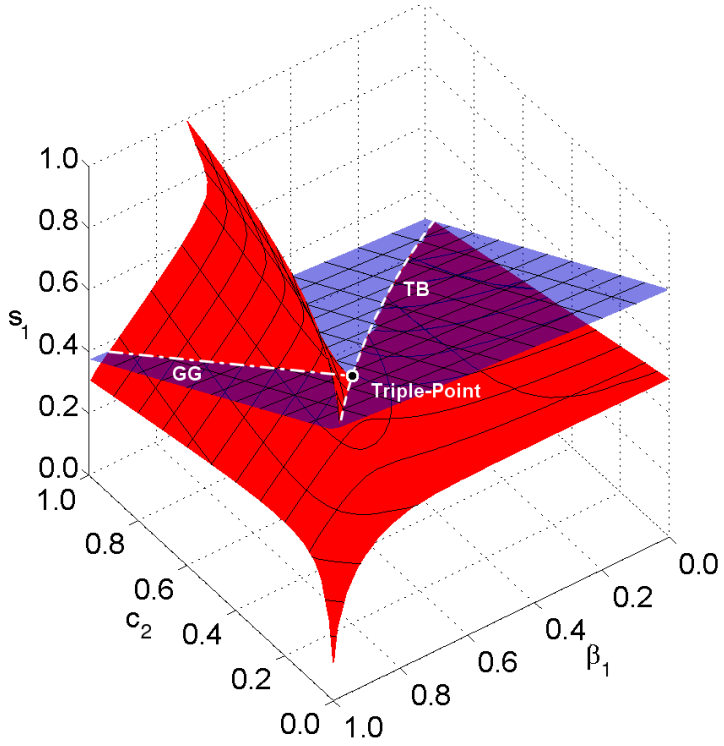

Figure 5: Bifurcation diagram of a generalized socio-economic model of farmers, bandits and rulers. The parameter β_1 is the fraction of farmer losses caused by crime. The other parameters s_1 and c_2 representing the availability of usable land and the autonomy of the bandits respectively. The red surface is a manifold of Hopf bifurcations and the slightly transparent blue surface is a manifold of saddle-node bifurcations. The stitched lines mark a Gavrilov-Guckenheimer (GG) and a Takens-Bogdanov (TB) bifurcation. The intersection point of these lines is a triple point bifurcation.

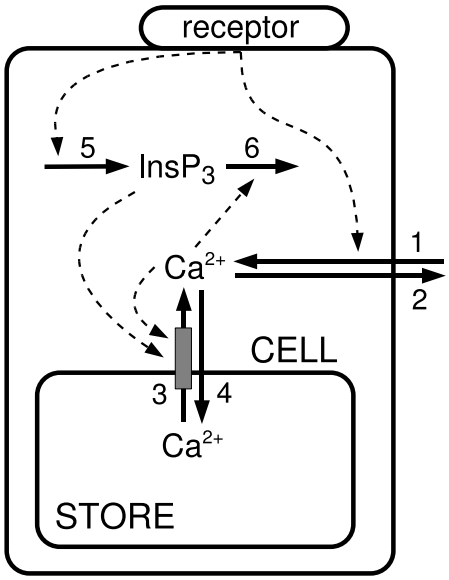

Figure 6: A minimal model of intracellular calcium dynamics [Houart et al., 1999]. The system consists of 3 concentration variables: cytoplasmic calcium Ca^{2+}_{cyt} and stored calcium Ca^{2+}_{store}, as well as cytoplasmic inositol 1,4,5-triphosphate ($InsP_3$). Release of Ca^{2+} from the internal store is controlled by a $InsP_3$-sensitive channel, as well as by cytoplasmic calcium itself (calcium-induced calcium release, CICR). The dynamics of the system are described by a set of 3 differential equations.

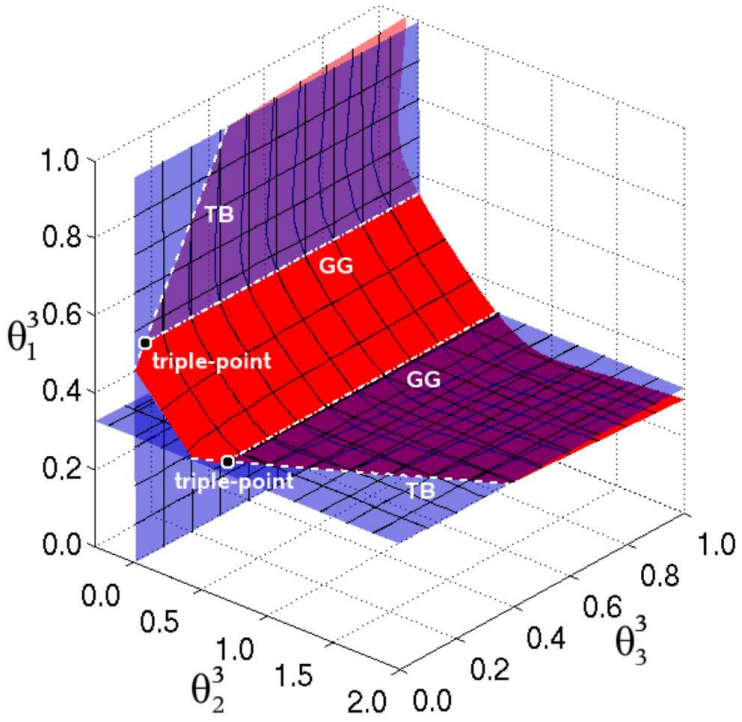

Figure 7: Bifurcation diagram of a metabolic network model of calcium oscillations. The red surface is a manifold of Hopf Bifurcations and the slightly transparent blue surfaces are manifolds of general saddle-node bifurcations. The dashed lines denote a Gavrilov-Guckenheimer bifurcation (GG) and a Takens-Bogdanov (TB) bifurcation. The intersection points of these lines are triple point bifurcations. Concentration and flux values, as well as all other saturation parameters are assumed to be constant, corresponding to the values found in [Houart et al., 1999]: $X_1^* = 0.35$, $X_2^* = 0.9$, $X_3^* = 0.13$ (in arbitrary units) and $\theta_1^2 = 0.15$, $\theta_1^6 = 0.25$, $\theta_3^6 = 0.8$.

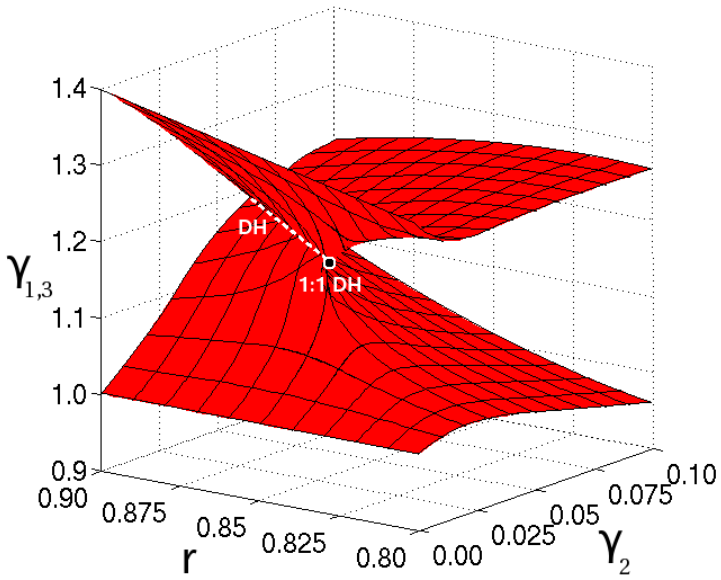

Figure 8: Bifurcation diagram of a four-trophic food chain. The value of r describes the ratio between the characteristic timescale of a predator and its prey, while $\gamma_{1,3} = \gamma_1 = \gamma_3$ and γ_n describes the sensitivity of predator X_{n+1} to its prey X_n. The red surface is a manifold of Hopf bifurcations that intersects with itself in a double Hopf bifurcation line (DH) of codimension 2, which is shown as a dashed line. The end of this line is a 1:1 resonant double Hopf bifurcation (1:1 DH) of codimension 3.